ELSEVIER

Polymer 42 (2001) 10063–10070

polymer

www.elsevier.com/locate/polymer

Preparation and crystallization behavior of syndiotactic polystyrene–clay nanocomposites

Chen-Rui Tseng[a], Jeng-Yue Wu[b], Hsin-Yi Lee[c], Feng-Chih Chang[a,*]

[a]*Institute of Applied Chemistry, National Chiao-Tung University, Hsin-Chu, Taiwan, ROC, 30043*
[b]*Department of Chemical Engineering, National Chung-Hsing University, Tai-Chung, Taiwan, ROC*
[c]*Synchrotron Radiation Research Center, Hsin-Chu, Taiwan, ROC*

Received 8 December 2000; received in revised form 7 May 2001; accepted 5 June 2001

Abstract

Syndiotactic polystyrene/modified-clay nanocomposites have been prepared by solution blending by mixing pure s-PS and organophilic clay with adsorbed cetyl pyridium chloride (CPC) in dichlorobenzene. The dispersability of the clay in syndiotactic polystyrene/modified-clay nanocomposites was studied using X-ray and transmission electron microscopy. The clay is well dispersed into the s-PS matrix using solution blending with scale in 1–2 nm or in a few tenths ~100 nm depending on surfactant treatment. The CPC is partially compatible with s-PS and allows syndiotactic polystyrene chains intercalating into clay layers. The crystallization behavior of α- and β-crystals for syndiotactic polystyrene nanocomposite has been thoroughly examined using the Fourier transform infrared and differential scanning calorimetry. Our results further demonstrate that the presence of the clay plays a vital role in facilitating the formation on the thermodynamically more favorable β form crystal when the s-PS is melt- or cold-crystallized. © 2001 Elsevier Science Ltd. All rights reserved.

Keywords: Syndiotactic polystyrene; Clay; Nanocomposites; Surfactant

1. Introduction

Inorganic particles have been widely used as reinforcement materials for polymers. Special attention has been paid to clay minerals in the field of nanocomposites due to its nano-scale size and intercalation properties [1]. There are two main approaches which suggest that polymer is intercalated into the silicate layers of clay mineral. One is the insertion of a suitable monomer and subsequent polymerization. The other is the direct insertion of polymer chains from solution or melt state. Silicate layers well dispersed in nylon 6 matrix have been accomplished by the first method [1,2]. This nylon hybrid exhibits superior properties such as high strength, high modulus and high heat distortion temperature compared to the virgin nylon 6 [3,4]. Poly(ι-lactide) (PLLA)-clay and poly (ϵ-caprolactone) (PCL)-clay blends were studied using the smectite-type clay-Montmorillonite as reinforcement [5,6]. Enhanced properties of the hybrid depend on the degree of clay dispersion within the polymer matrix. However, the hydrophilic nature of clay does not afford its good dispersion in organic polymer phase. It is essential to improve the interaction between clay and polymer matrix to produce a useful polymer nanocomposite.

Syndiotactic polystyrene (s-PS) is a newly synthesized engineering thermoplastic [7,8]. The s-PS differs from the atactic or isotactic polystyrene in that, the phenyl rings regularly alternate from side to side with respect to the zig-zag polymer chain backbone and this regular structure allows s-PS to crystallize readily. The extent to which the thermal history affects the crystalline structure and crystallization kinetics for s-PS has been studied extensively [9–12]. Typically, α- and β-crystals can be obtained by melt- and cold-crystallizations, and the β-crystal is considered to be favored over the α-crystal in the s-PS at higher temperature of crystallization [13,14]. This s-PS possesses high melting temperature (~270°C), high stiffness and good solvent resistance that has attracted many researchers to study its structure and properties [15–17]. In recent years, organic–inorganic nanometer composites have evolved and attracted great interests from industries and academics. At least two important factors need to be considered to achieve the homogeneous dispersion of the clay layers in the s-PS hybrids. First, the surfactant

* Corresponding author. Tel.: +886-3-5712121, ext.: 56502; fax: +886-3-5723764.
E-mail address: changfc@cc.nctu.edu.tw (F.-C. Chang).

0032-3861/01/$ - see front matter © 2001 Elsevier Science Ltd. All rights reserved.
PII: S0032-3861(01)00568-7

should be intercalated between silicate layers of clay through ionic bonding. Secondly, the hydrophobic tail of the surfactant molecule should be partially compatible or interacted with s-PS molecules.

Fourier transform infrared (FTIR) spectroscopic techniques have been extensively applied to assess polymer crystallinity and chain conformation. As a highly effective means of characterizing polymers structurally, FTIR complements other techniques in providing detailed information about chain conformation changes and the crystallinity of crystalline polymers, that is nondestructive and fast [18].

This study prepares s-PS/clay nanocomposites using polymer intercalation from solution. Both transmission electron microscopy (TEM) and X-ray are used to characterize clay dispersibility in the s-PS matrix. Solid state FTIR is used to characterize the changes of crystalline form and crystallinity in the clay containing s-PS. Isothermal differential scanning calorimetric (DSC) analyses are also conducted to examine the effect of clay content on crystallization behavior of the s-PS/clay nanocomposites.

2. Experimental

2.1. Materials

Montmorillonite 'Kunipia F' was supplied by the Kunimine Co. of Japan. This clay mineral bears exchangeable sodium ions with cation exchange capacity (CEC) of ca. 119 meq per 100 g. The s-PS was kindly supplied by the Industrial Technology and Research Institute (ITRI) of Taiwan, which was synthesized using a homogeneous catalyst consisting of $CpTiCl_3$ and methylalumoxane (MAO) in toluene [19], with $M_n = 100,000$. The chemical structure of the syndiotactic polystyrene with [rr] = 99% has been identified by the solution ^{13}C NMR spectrum. Cetyl pyridium chloride, a cationic surfactant, was purchased from Sigma with purity greater than 99%.

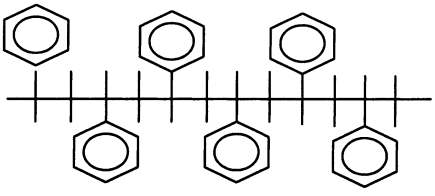

syndiotactic polystyrene

cetyl pyridium chloride

2.2. Preparation of organophilic clay mineral

Sodium montmorillonite (1 g) and 50 ml of distilled water were placed in a 100 ml beaker, 0.39 g of cetyl pyridium chloride (CPC) was added to the solution (clay/CPC = 1/1). The mixture was stirred vigorously for 8 h and then filtered and washed with deionized water. The product was freeze-dried in a vacuum oven at room temperature for 24 h. The organophilic clay mineral thus obtained is highly hydrophobic.

2.3. Preparation of s-PS/clay–CPC hybrids

Pre-weighed amount of the well-dried organically modified monmorillonite and the s-PS powder were placed in a beaker, the hot dichlorobenzene was added and the solution kept at 140°C under constant agitation for 24 h. The product was freeze-dried and kept in a vacuum oven at 140°C for another 24 h. A translucent film was obtained when the dichlorobenze was vaporized.

2.4. Characterizations

2.4.1. Wide-angle X-ray diffraction

X-ray diffraction spectra were collected on an X-ray diffraction instrument (M18XHF-SRA., MacScience Co., Japan) using the CoKα radiation, and the Bragg's Law ($\lambda = 2d \sin\theta$) was used to compute the spacing.

2.4.2. Transmission electron microscope

Transmission electron micrographs were taken from a microtoned section of s-PS/clay hybrids of 60 ~ 100 nm thickness mounted in epoxy using a TEM (JEM-2000FX, Joel Co., Japan) with an acceleration voltage of 100 kV.

2.4.3. Differential scanning calorimeter isothermal crystallization

Differential scanning calorimeter (DSC 2010, Du Pont) was used for determining the melting transition temperature and melting enthalpy of the s-PS. The s-PS/clay–CPC hybrid with about 5–10 mg in an alumna pan was heated in DSC furnace to 320°C and kept at that temperature for 10 min to ensure total relaxation of the sample and to eliminate the influence of thermal history. Isothermal cold- and melt-crystallization of s-PS/clay–CPC hybrids were performed in an environmental chamber equipped with a temperature programmable controller to an accuracy of ±0.1°C. For melt-crystallization, the s-PS/clay–CPC hybrid was heated to 320°C for 10 min and quickly cooled (−100°C/min) to 240°C for 10 min, and then heated from 240 to 310°C with a heating rate of 10°C/min to obtain the melting transition temperature and melting enthalpy of the s-PS. For cold-crystallization, the s-PS/clay–CPC hybrid quenched by liquid nitrogen from 320°C for 10 min was placed directly into the DSC chamber at 240°C, isothermally for 10 min, and then heated from 240 to 310°C with

Table 1
The DSC data of s-PS/CPC blending

s-PS content (%)	CPC content (%)	T_g (°C)
100	0	97.0
99	1	53.4
97	3	48.7
95	5	17.1
90	10	12.5

a heating rate of 10°C/min to obtain the melting transition temperature and melting enthalpy of s-PS.

2.4.4. Infrared spectra

Infrared spectra ranging from 4000–400 cm^{-1} were obtained at a resolution of 1.0 cm^{-1} with FTIR (Nicolet AVATAR 320 FTIR spectrometer, USA), at 30°C. The frequency scale was internally calibrated using a He–Ne laser and 32 scans were single-averaged to reduce the noise. The crystal form determination of the s-SP/clay–CPC hybrid by FTIR was carried out in both melt- and cold-crystallization at 240°C and then quenching by liquid nitrogen. The thickness of s-PS sample is controlled at less than 10 μm to minimize the effect of thickness on crystallization. All sample preparations were under continuous nitrogen flow to ensure minimal sample oxidation or degradation.

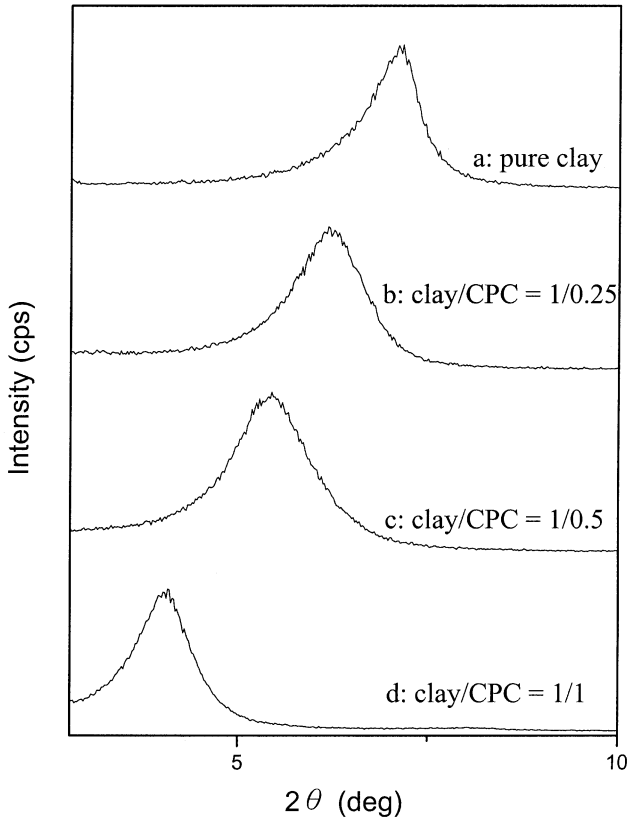

Fig. 1. X-ray diffraction patterns ranging from $2\theta = 3$ to 10° for untreated and CPC treated clay.

3. Results and discussion

3.1. Miscibility of s-PS/CPC hybrid

Table 1 shows the DSC data of s-PS/CPC blends by solution blending using dichlorobenzene as the solvent. The T_g of the pure s-PS is 97°C, and decreases to 12.5°C when the CPC content is increased up to 10 wt%. Single T_g had been observed up to 10% of the CPC. The s-PS and CPC are miscible with CPC content up to 10% and CPC can be considered as a plasticizer for s-PS.

The XRD patterns of various clay/CPC ratios are shown in Fig. 1. The XRD pattern (Fig. 1(a)) of the unmingled clay shows basal reflections characteristic of $2\theta = 7.1°$ (basal spacing ~1.2 nm). The layer spacing of the clay increases with an increasing CPC content as shown in Fig. 1(b)–(d). When the clay/CPC ratio is 1/1, the basal reflection is around $2\theta = 4°$ (basal spacing ~2.2 nm). This result indicates that the CPC is indeed intercalated into the layers of clay. Notably, the difference in compatibility between clay and clay/CPC with s-PS significantly affects the formation of layered structure in the nanoscale level. The s-PS chains can be more easily intercalated into the narrow space of the oriented collections of parallel silicate layers by CPC pretreatment. It is reasonable to assume that the presence of CPC is able to enhance the diffusion of the s-PS chains into the silicate interlayers.

3.2. Dispersibility of clay in s-PS/clay–CPC hybrids

Degrees of clay dispersion in s-PS/clay–CPC hybrids can be judged from the XRD patterns. Fig. 2 shows XRD patterns of various s-PS/clay–CPC hybrids where the clay was modified by equivalent exchanged moles of CPC (i.e. clay/CPC = 1/1 by mole). The peak of clay/CPC = 1/1 is around $2\theta = 4°$. The addition of s-PS to the clay/CPC hybrid, shifts the XRD reflection peak to lower angles. The interlayer spacing of s-PS/clay–CPC = 5/95 is very close to that of the modified clay/CPC = 1/1, compared (Fig. 2(a) and (b)). This result indicates that the 5% s-PS chain is insignificant to cause further intercalation of the silicate layers. The clay layers still maintain a relative ordering of the layered structures in the s-PS/clay–CPC = 5/95 hybrid as well as in the clay/CPC = 1/1. The interlayer spacing of the clay in this s-PS/clay–CPC = 20/80 hybrid is around 2.7 nm (Fig. 2(c)) and the s-PS/clay–CPC = 80/20 hybrid is around 3.1 nm (Fig. 2(e)). Clearly, basal space of clay interlayers is dependent on the amount of the added s-PS. There is no apparent peak of the clay that can be detected in the s-PS/clay–CPC = 95/5 hybrid (Fig. 2(f)) indicating that the exfoliation of clay is more severe than others. The diffraction peak ($2\theta = 6.3°$) shown in Fig. 2(f) comes from the s-PS β-crystals

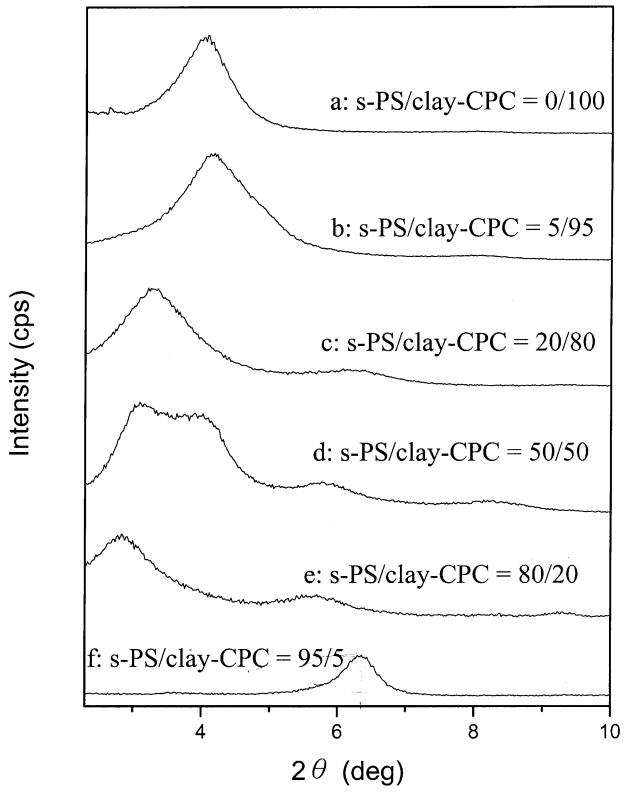

Fig. 2. X-ray diffraction patterns ranging from $2\theta = 2$ to 9° for various s-PS/clay-CPC hybrids with clay/CPC = 1/1.

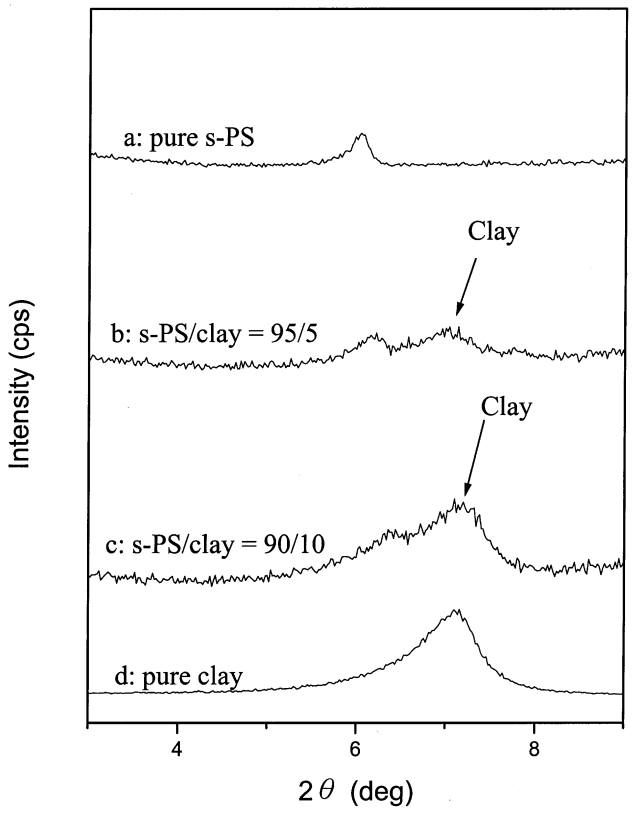

Fig. 3. X-ray diffraction patterns ranging from $2\theta = 3$ to 10° for (a) pure s-PS; (b) s-PS/clay = 95/5; (c) s-PS/clay = 90/10; and (d) pure clay.

(Fig. 3(a)) [18,20,21]. The basal spacing of the clay increases progressively with increasing s-PS content in the s-PS/clay–CPC hybrid.

Fig. 3 shows the XRD patterns of neat s-PS, neat clay and various s-PS/neat clay compositions. The X-ray diffraction pattern of the pure clay contains basal reflections that are characteristic of un-intercalated repeat distance of $d = 1.2$ nm ($2\theta = 7.1°$) as shown in Fig. 3(d). One sharp peak, $2\theta = 6.3°$, appears in Fig. 3(a) which corresponds to the β-form s-PS crystal. Two peaks, $2\theta = 7.1$ and 6.3° shown in Fig. 3(b) and (c) correspond to pure clay and β-form s-PS crystal, respectively. The reflection peaks of clay are widened in both s-PS/clay = 95/5 and 90/10 while their peak locations remain unchanged at around 7.1°. Therefore, the basal space of the clay does not change in both samples when the clay is not treated by CPC. This means that the initial intercalation of small amount of the CPC is necessary to bring in the s-PS chains, diffusing into silicate layers.

In order to further elucidate the effect of CPC on hybrid structures and on the dispersion of silicate layers, samples of s-PS/clay = 95/5 hybrids, with and without CPC (clay/CPC = 1/1), are examined using TEM as shown in Fig. 4. Fig. 4(a) shows the TEM bright field image of the s-PS/clay–CPC hybrid, where the dark lines denote the silicate layers. The surfactant CPC accommodates the intercalated clay by the organic cation and renders the hydrophobic silicate surface organophilic. The stacked silicate layers of about 1–5 nm thickness (about 1–3 parallel silicate layers), are randomly distributed in the s-PS matrix. Fig. 4(b) reveals that the untreated clay in the s-PS matrix is not well dispersed, indicating that the layers of clay are not exfoliated. The clay layers shown in Fig. 4(b) are relatively rougher and more agglomerated than those shown in Fig. 4(a). These observations correlate well with the XRD patterns. The presence of CPC surfactant in clay significantly affects the dispersibility of the silicate layers in the s-PS/clay hybrid.

3.3. Effects of clay on crystal form and crystallinity for s-PS

Fig. 5 presents the FTIR spectra of neat s-PS and s-PS/clay–CPC hybrids with different clay/CPC contents prepared by solution blending. To clearly understand the change caused by adding different amounts of the clay/CPC = 1/1, the IR spectra are taken from 940 to 820 cm^{-1}, which are highly sensitive to chain packing for the s-PS polymorph [22–24]. The characteristic infrared bands at 905 and 841 cm^{-1} originate from the amorphous phase of the s-PS [13,14]. As is well-known, the thermodynamically favored β-form of the s-PS is more preferably formed through melt-crystallization at a high temperature [13,14]. The newborn bands appearing at 911 and 858 cm^{-1}

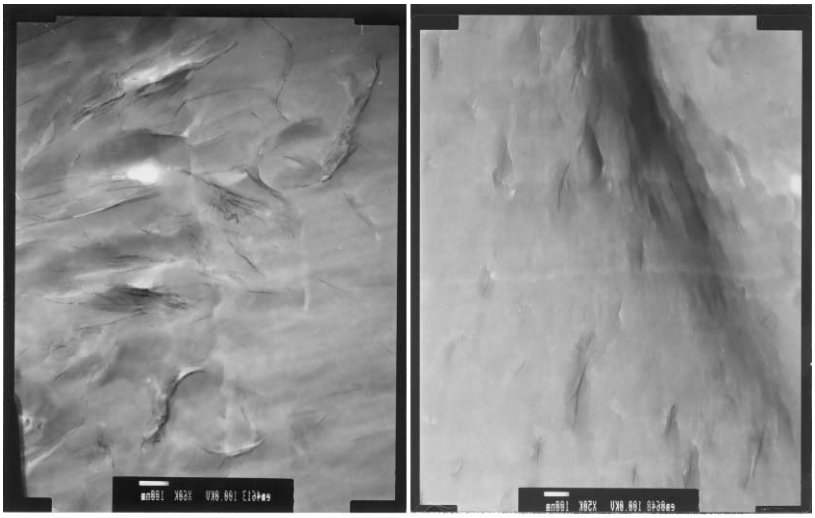

(a) (b)

Fig. 4. TEM micrographs of thin sections of (a) s-PS/clay–CPC = 95/5 with clay/CPC = 1/1; and (b) s-PS/clay = 95/5 hybrid obtained from solution blending without thermal treatment.

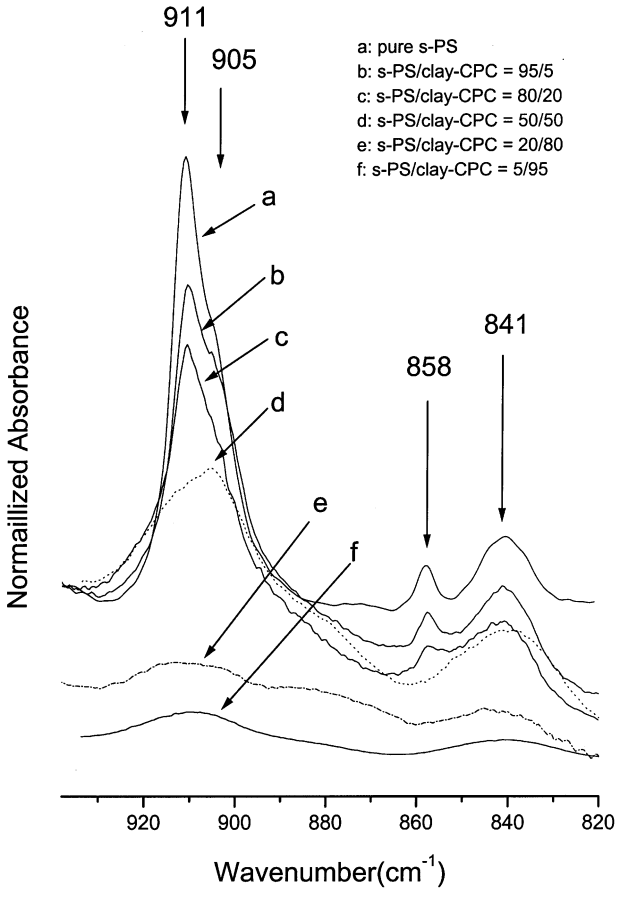

Fig. 5. FTIR spectra of melt-crystallized isothermally at 240°C for pure s-PS and various s-PS/clay-CPC hybrids with clay/CPC = 1/1.

correspond to the β-crystal when the s-PS is melt-crystallized at 240°C for 10 min and then quenched by liquid nitrogen. The characteristic peaks of the α-crystal are absent in Fig. 5(a). Fig. 5 reveals that the intensity of the β-crystal phase peaks (911 and 858 cm^{-1}) for the s-PS/clay–CPC hybrid prepared by solution blending decreases with increasing clay/CPC content (Fig. 5(b)–(f)). In the s-PS/clay–CPC = 50/50 hybrid, the amorphous phase peak of the s-PS (905 cm^{-1}) is larger than that of the β-crystal phase peak (911 cm^{-1}) as shown in Fig. 5(d). The characteristic peaks of the β-crystal (911 and 858 cm^{-1}) are absent when the addition of the clay/CPC is 95%, indicating that the s-PS chains in s-PS/clay–CPC = 5/95 hybrid do not crystallize (Fig. 5(f)).

Fig. 6 shows the DSC thermograms of these annealed samples obtained with a heating rate of 10°C/min from 240 to 310°C, after melt-crystallization at 240°C for 10 min. Table 2 summarizes the thermodynamic parameter of these melt-crystallized s-PS/clay–CPC hybrids obtained from Fig. 6. This special heating scan program can avoid re-crystallization at a lower scanning temperature, the actual melt point (T_m) and melt enthalpy (ΔH_m) of the s-PS can be obtained from these DSC scans. The melt-crystallized pure s-PS at 240°C contains one major melting peak at ~271°C and one minor melting peak at ~259°C (Fig. 6(a)). The major and minor melting peaks correspond to the melting of the originally packed thick and thin β-crystal lamella, respectively [13,14]. Comparing the T^{β}_{m1} and T^{β}_{m2}, reveals that the perfection of crystals of the pure s-PS in the thick lamellae is higher than that in the thin lamellae. However, in s-PS/clay–CPC hybrid prepared by solution blending, part of the thick β-crystal phase peak (~271°C) shifts to ~265°C (T^{β}_{m3}) as shown in Fig. 6(b)–(d). It is proposed that the highly dispersive clay, intercalated by s-PS chains, tends

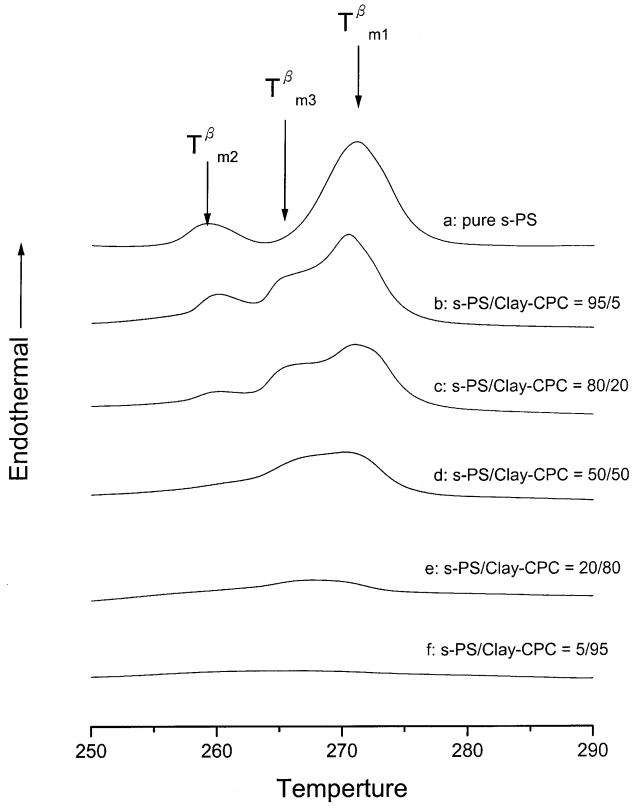

Fig. 6. DSC thermograms with scan rate of 10°C/min after isothermal melt-crystallization at 240°C for 10 min for pure s-PS and various s-PS/clay-CPC hybrids with clay/CPC = 1/1.

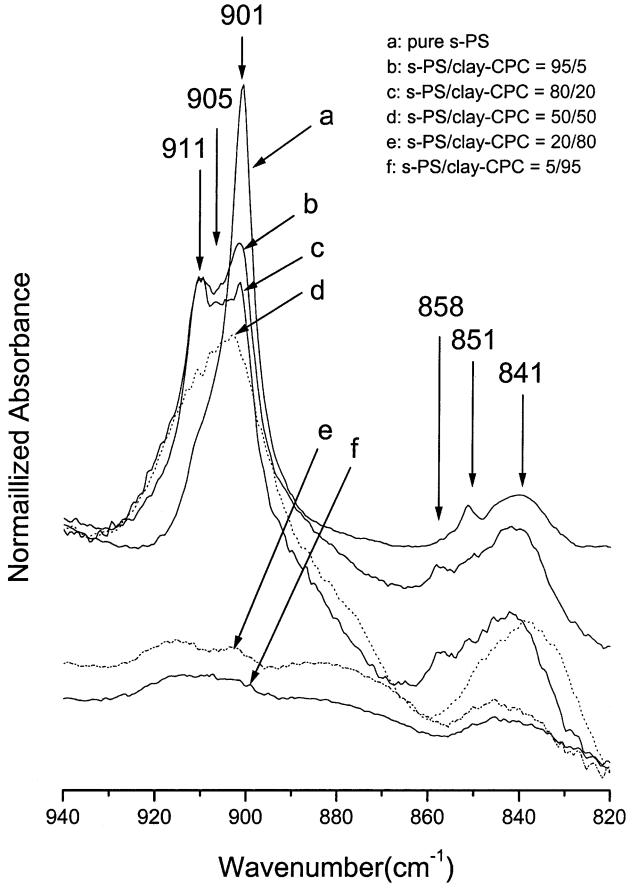

Fig. 7. FTIR spectra of cold-crystallized isothermally at 240°C for pure s-PS and various s-PS/clay-CPC hybrids with clay/CPC = 1/1.

to increase the number of 'initial nuclei' and forms the β-crystal lamellae with different nucleus size in melt-crystallization, at 240°C. It has been clearly demonstrated that the presence of clay/CPC employed significantly affect the nucleus size associated with the morphology of the s-PS. This observation suggests that the clay/CPC changes the conventional mechanism of molecular packing of the neat s-PS. Fig. 6(f) reveals that the β-crystal lamellae nearly disappears when the amount of the clay/CPC is 95% of the s-PS matrix. These observations also correlate well with the FTIR spectra.

Table 2
The thermodynamic parameter of melt-crystallized for s-PS/clay-CPC hybrids obtained from Fig. 6

Composition (%)	Melting point (°C)			Melting enthalpy, ΔH_m (J/g)	Ratio[a] (%)
	T^{β}_{m1}	T^{β}_{m3}	T^{β}_{m2}		
Neat s-PS	271.7	–	259.8	23.7	100.0
s-PS/clay–CPC = 95/5	270.5	265.0	260.0	22.8	96.2
s-PS/clay–CPC = 80/20	271.1	265.3	259.9	19.2	81.0
s-PS/clay–CPC = 50/50	270.4	267.1	–	8.95	37.8
s-PS/clay–CPC = 20/80	267.6	–	–	3.40	14.3
s-PS/clay–CPC = 5/95	–	–	–	–	–

[a] Ratio (%) = $\Delta H_m/\Delta H^0_m$ where ΔH^0_m is the melting enthalpy of neat s-PS.

Fig. 7 shows the FTIR spectra from the cold-crystallized s-PS and s-PS/clay–CPC hybrids at 240°C, for different clay/CPC contents, prepared by solution blending. The FTIR change of the pure s-PS shown in Fig. 7(a) is not as severe as that in Fig. 5(a). The newborn bands appearing at 901 and 851 cm^{-1} correspond to the α-crystal when the s-PS is cold-crystallized at 240°C for 10 min and then quenched by liquid nitrogen [14]. The β-crystal phase peaks (911 and 858 cm^{-1}) are absent in the cold-crystallized pure s-PS sample (Fig. 7(a)). There is a manifestation that at 240°C, the crystallization of the α-crystal approaches the stable state faster than that of the β-crystal. However, the intensities of the α-crystal peaks (901 and 851 cm^{-1}) are decreased with increasing the clay/CPC content; while intensities of the β-crystal peaks (911 and 858 cm^{-1}) are increased (Fig. 7(b) and (c)). This result indicates that the crystal transformation from α- to β- occurs by the addition of clay/CPC to the s-PS matrix during the process of cold-crystallization. Better clay dispersion in s-PS matrix lowers the potential energy of the β-crystal phase in the initial stage of molecular reorder and the s-PS chains can be intercalated more efficiently into the silicate layers of the clay to form the thermodynamically more favorable β-form of the s-PS. Fig. 7(e) and (f) reveal that the

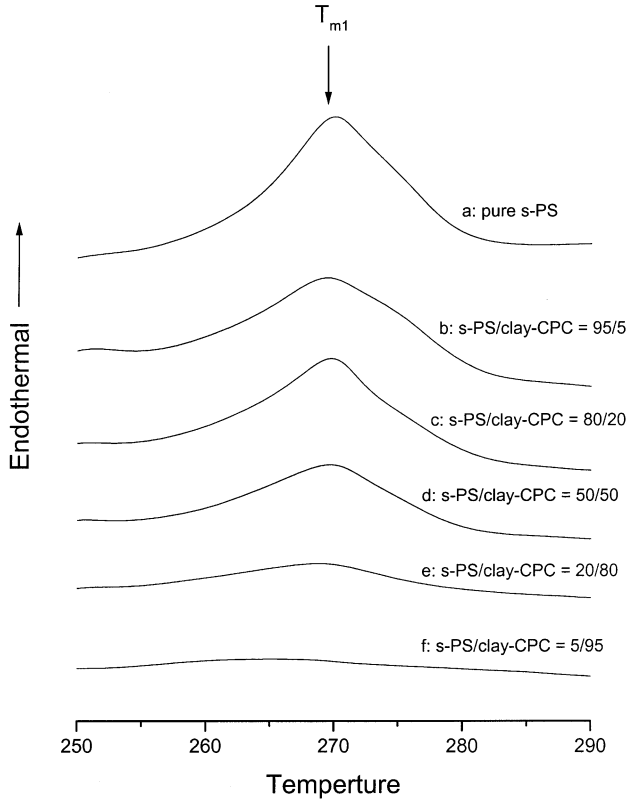

Fig. 8. DSC thermograms with scan rate of 10°C/min after isothermal cold-crystallization at 240°C for 10 min for pure s-PS and various s-PS/clay-CPC hybrids with clay/CPC = 1/1.

crystal lamellae nearly disappears and the amorphous phase dominates when the amount of the clay/CPC is 80 or 95% in the s-PS matrix.

Fig. 8 shows the corresponding DSC thermograms of these cold-crystallized s-PS and s-PS/clay–CPC hybrids obtained with a heating rate of 10°C/min from 240 to 310°C. Table 3 summarizes the thermodynamic parameter of these cold-crystallized s-PS/clay-CPC hybrids obtained from Fig. 8. The s-PS and s-PS/clay–CPC hybrids upon DSC scanning from 240 to 310°C after cold-crystallization show a round-shaped melting peak and their melting points (T_m) remain almost a constant. In cold-crystallization, the melting point (T_m) and its enthalpy of melting (ΔH_m), come from α- and β-crystal phases of the s-PS. The decrease in the enthalpy of melting (ΔH_m) for the s-PS, can be associated with the increase in the clay/CPC content. This result correlates well with that from the melt-crystallization.

Table 3
The thermodynamic parameter of cold-crystallized for s-PS/clay–CPC hybrids obtained from Fig. 8

Composition (%)	T_m (°C)	Melting enthalpy, ΔH_m (J/g)	Ratio[a] (%)
Neat s-PS	269.9	19.0	100.0
s-PS/clay–CPC = 95/5	269.7	18.3	96.3
s-PS/clay–CPC = 80/20	269.8	17.1	90.0
s-PS/clay–CPC = 50/50	269.8	7.94	41.8
s-PS/clay–CPC = 20/80	269.3	3.58	18.8
s-PS/clay–CPC = 5/95	–	–	~0

[a] Ratio (%) = $\Delta H_m/\Delta H_m^0$ where ΔH_m^0 is the melting enthalpy of neat s-PS.

4. Conclusions

In this study, s-PS nanocomposites have been successfully prepared by solution blending. The miscibility between the surfactant and the s-PS is essential to disperse the clay layers into the s-PS matrix. Experimental results indicate that s-PS chains can intercalate more efficiently into the silicate layers when clay is pretreated with CPC surfactant. The crystal form and crystallinity of s-PS matrix with the clay/CPC are investigated by the FTIR spectra and DSC thermograms. Results from this study demonstrate that during melt-crystallization, the better dispersibility of the clay in the s-PS matrix changes the nucleus size of β-crystal lamellae for the s-PS. As a matter of fact, the cold-crystallized s-PS shows exclusive α-crystal but the crystal transformation from α- to β occurs by adding clay/CPC into the s-PS matrix. The addition of clay in the s-PS matrix lowers the potential energy of the β-crystal of s-PS chains, during cold-crystallization and thus provides a new pathway to generate β form crystal in the s-PS matrix. This finding suggests that the presence of clay/CPC changes the conventional mechanism of molecular packing for the s-PS.

Acknowledgements

The authors would like to thank the National Science Council of the Republic of China for financially supporting this research under Contract No. NSC-88-2116-E-009-006.

References

[1] Vaia RA, Ishii H, Giannelis EP. Chem Mater 1993;5:1694.
[2] Usuki A, Kojima Y, Kawasumi M, Okada A, Fukushima Y, Kurauchi T, Kamigaito O. J Mater Res 1993;8:1179.
[3] Kojima Y, Usuki A, Kawasumi M, Okada A, Fukushima Y, Kurauchi T, Kamigaito O. J Mater Res 1993;8:1185.
[4] Kojima Y, Usuki A, Kawasumi M, Okada A, Kurauchi T, Kamigaito O. J Appl Polym Sci 1993;49:1259.
[5] Ogata N, Jimenez G, Kawai H, Ogihara T. J Polym Sci B: Polym Phys 1997;35:389.
[6] Jimenez G, Ogata N, Ogihara T. J Appl Polym Sci 2001, in press.
[7] Ishihara N, Seimiya T, Kuramoto N, Uoi M. Macromolecules 1987;19:2464.
[8] Ishihara N, Seimiya T, Kuramoto N, Uoi M. Eur Pat Appl 1987;210:615.
[9] Nakaoki T, Kobayashi M. J Mol Struct 1991;242:315.
[10] Reynolds NM, Stidham HD, Hsu SL. Macromolecules 1991;24:3662.
[11] Guerra G, Vitagliano VM, De Rosa C, Petraccone V, Corradini P. Macromolecules 1990;23:1539.
[12] Kobayashi M, Nakaoki T, Ishihara N. Macromolecules 1989;22:4377.
[13] Wu HD, Wu ID, Chang FC. Macromolecules 2000;33:8915.

[14] Wu HD, Wu SC, Wu ID, Chang FC. Polymer 2001;42:4719.
[15] Wesson RD. Polym Engng Sci 1994;34:14.
[16] Krzystowczyk DH, Niu X, Wesson RD, Collier JR. Polym Bull 1994;33:109.
[17] Cimmino S, Pace ED, Martuscelli E, Silvestre C. Polym Commun 1991;32:251.
[18] Wu HD, Tseng CR, Chang FC. Macromolecules 2001;34:2992.
[19] Pellecchia C, Longo P, Grassi A, Ammendola P, Zambelli A. Makromol Chem Rapid Commun 1987;8:277.
[20] Kojima Y, Usuki A, Kawasumi M, Okada A, Fukushima Y, Kurauchi T, Kamigaito O. Mater Res 1993;8:1185.
[21] De RC, Corradini P. Macromolecules 1993;26:5711.
[22] Pellecchia C, Longo P, Grassi A, Ammendola P, Zambelli A. Makromol Chem Rapid Commun 1987;8:277.
[23] Musto P, Tavone S, Guerra G, De Rosa C. J Polym Sci B: Polym Phys 1997;35:1055.
[24] Vittoria V, Ruvolo Filho A, De Candia F. J Macromol Sci Phys B 1990;29:411.